

# We are IntechOpen, the world's leading publisher of Open Access books Built by scientists, for scientists

6,900

Open access books available

186,000

International authors and editors

200M

Downloads

Our authors are among the

154

Countries delivered to

TOP 1%

most cited scientists

12.2%

Contributors from top 500 universities



WEB OF SCIENCE™

Selection of our books indexed in the Book Citation Index  
in Web of Science™ Core Collection (BKCI)

Interested in publishing with us?  
Contact [book.department@intechopen.com](mailto:book.department@intechopen.com)

Numbers displayed above are based on latest data collected.  
For more information visit [www.intechopen.com](http://www.intechopen.com)



---

# Heat Treatment in Molecular Precursor Method for Fabricating Metal Oxide Thin Films

---

Hiroki Nagai and Mitsunobu Sato

Additional information is available at the end of the chapter

<http://dx.doi.org/10.5772/50676>

---

## 1. Introduction

Industrial processes must minimize heat-treatment to reduce energy consumption and CO<sub>2</sub> emissions during the manufacture of products. In particular, fossil fuels should be conserved for the next generation. However, the use of heat-treatment is essential in the manufacturing processes of many highly functional materials.

In many cases, the materials' functions depend on their surfaces. From this point of view, modification by thin film fabrication on various substrates, as opposed to manufacturing the entire body with the functional material, can generally save resources. The molecular precursor method (MPM) that was developed in our study is a wet chemical process for fabricating metal oxide and phosphate thin films [1-11]. This method requires heat-treatment to eliminate organic ligands from metal complexes involved in spin-coated precursor films and to fabricate thin films of crystallized metal oxides or phosphates. We emphasize the importance of heat-treatment by describing recent results obtained using the MPM, which show great potential for the development of nanoscience and nanotechnology tools and materials.

This chapter focuses on the transparent thin film fabrication of both a visible (Vis)-light-responsive anatase thin film having enhanced UV sensitivity and an unprecedented Vis-responsive rutile thin film on glass substrates. These photoreactive thin films were easily fabricated using the MPM. Heat-treatment under controlled conditions produced these attractive thin films. Thin film fabrication of a highly conductive Ag nanoparticles/titania composite and several metal oxides, including Cu<sub>2</sub>O, will be also discussed, illustrating the broad utility of the MPM and the importance of heat-treatment in this novel wet process.

## 2. Solution-based thin film formation

Novel thin films are an active area of research and are widely used in industry. Most of the thin films have thicknesses ranging from monolayer to nanometer levels up to several micrometers. Due to their relatively high hardness and inertness, ceramic coatings are of particular interest for the protection of substrate materials against corrosion, oxidation, and wear resistance [12-17]. The electronic and optical properties of thin films are used in many electronic and optical devices [18-20]. The wide range of materials, techniques for preparation, and range of applications make this an interdisciplinary field. Many different methods are used to fabricate thin films, including physical techniques and chemical processes. Physical vapor deposition (PVD) and chemical vapor deposition (CVD) are the two most common types of thin film formation methods. PVD methods such as thermal evaporation and sputtering involve atom by atom, molecule by molecule growth, or ion deposition on various materials in a vacuum system [21-23]. CVD and sol-gel methods are less expensive than PVD [24, 25]. The heat-treatment of thin films in these methods is generally important for the formation of crystallized metal oxides.

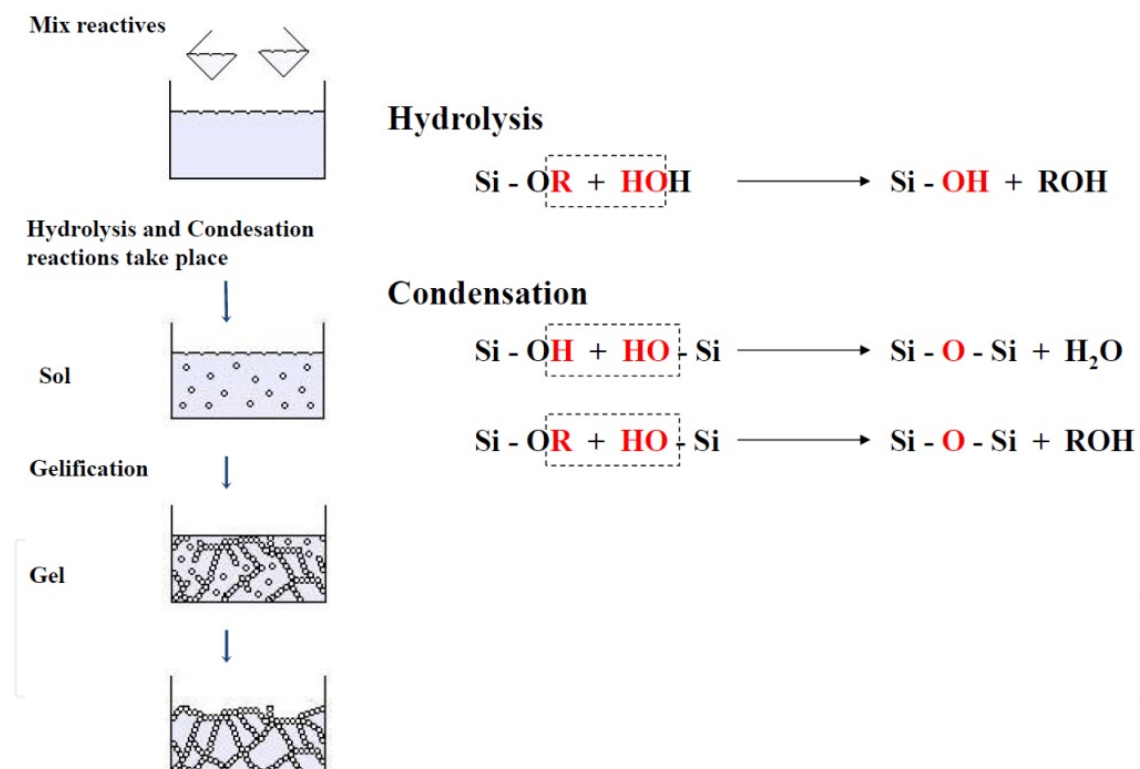


**Figure 1.** Typical sol-gel process for SiO<sub>2</sub> formation from silicone alkoxide.

The sol-gel method is a versatile technology in which metal/organic polymers are used to produce ceramics and glasses [26-34]. This technology can be used to manufacture thin films in a relatively cheap way compared with PVD. In a typical sol-gel protocol (Figure 1), the process starts with a solution consisting of metal compounds, such as a metal alkoxide, acetylacetonate, carboxylate, and soluble inorganic species as the source of cations in the target oxide. Additional reactants include water as the hydrolysis agent, alcohols as the

solvent, and an acid or base as a catalyst. Metal compounds undergo hydrolysis and polycondensation near room temperature, giving rise to a sol in which polymers or colloidal particles are dispersed without precipitation. Further reaction connects the fine particles, solidifying the sol into a wet gel, which still contains water and solvents. Vaporization of solvents and water produces a dry gel. Heating the gel to higher temperatures, where the organic constituents and residues are removed, gives rise to microstructures of inorganic-inorganic composites or hybrids, and glasses and ceramics. In Figure 2, the structural changes to metal oxides from the corresponding hydrolysed polymers by heat treatment of the as-deposited gel. The processes accompanied with dehydration can be categorized into two reactions; (A) the intrachain and (B) the interchain condensation.

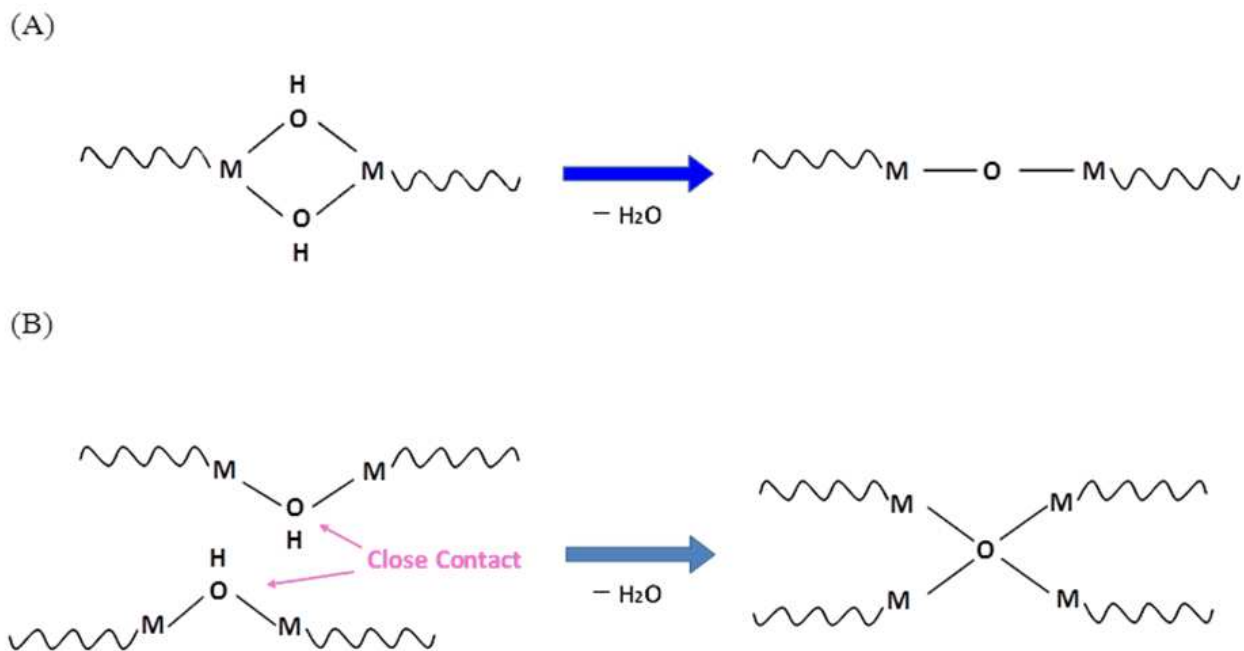


**Figure 2.** Plausible schematic diagrams for the oxide nucleation process of (A) intra-chain and (B) inter-chain condensation of the metalloxane polymers formed at the early stage in the sol-gel method.

### 3. Principle of MPM

The MPM is a wet process for the formation of thin films of various metal oxides, including titania or calcium phosphate compounds [1-11]. This method is based on the design of metal complexes in coating solutions with excellent stability, homogeneity, miscibility, coatibility, *etc.*, which have many practical advantages. This is because metal complex anions with high stability can be dissolved in volatile solvents by combining them with the appropriate alkylamines. Furthermore, the resultant solutions can form excellent precursor films through various coating procedures. The precursor films involving metal complexes should be amorphous, just as with the metal/organic polymers in the sol-gel processes. If not, it is impossible to obtain the resulting metal oxide thin films spread homogeneously on substrates by subsequent heat-treatment. For this purpose, the alkyl groups in the amines play an important role. Single-crystals of the metal complex can be obtained from the precursor solution in several cases when the alkyl groups in the alkylamines are sufficiently small, *e.g.*, an ethyl group. The model structure of the amorphous precursor films formed on substrates can be examined by means of crystal engineering and based on the crystal structures. Heat-treatment is necessary to fabricate the desired metal oxide films by eliminating the ligand in the metal complex and alkylamine as the counter cation. It is important that densification during heat-treatment occurs only in the vertical direction of the coated substrate.

To the best of our knowledge, the crystallite size of the oxide particles in the resultant thin films fabricated by the MPM is generally smaller than those prepared by the conventional sol-gel method. The smaller size of the crystallites obtained using the MPM may be related to the nucleation process of the crystallized metal oxides. In the nucleation process in the sol-gel method, the polymer chains themselves are rearranged by heat-treatment (Figure 2). The polymer chains should move to produce the core structure of the metal oxide, especially during interchain condensation. In contrast, the nucleation of metal oxides occurs more easily during the MPM. When coupled with elimination of the organic ligands via heat-treatment, a vast number of crystallites can be rapidly formed. It is consequently feasible that the crystallite sizes of metal oxides fabricated using the MPM are smaller than those obtained using the sol-gel method.

## 4. Heat-treatment for titania thin film fabrication

### 4.1. Thin film fabrication and basic properties of TiO<sub>2</sub>

Titania is a popular industrial material that has been used as a white pigment for paints, cosmetics, and foodstuffs [35]. The photoreactivity of titania is known from observations of phenomenon such as the chalking of white paints containing titania after long-term outdoor exposure. The photoreactivity of titania was first observed by Honda and Fujishima in 1967, and reported in the literature in 1972 [36]. When the surface of a titania electrode (under an appropriate bias between a Pt counter electrode) was irradiated with light of energy shorter than its band gap, 3.0 eV, a photocurrent flowed from the Pt electrode to the titania

electrode through the external circuit. The oxidation reaction occurs at the titania electrode, and the reduction reaction occurs at the Pt electrode. This observation showed that water molecules could be split into oxygen and hydrogen using UV light in a sulfuric acid electrolyte. The energy-conversion process that occurs on the titania surface is termed the Honda–Fujishima effect. When titania particles absorb UV radiation, they produce pairs of electrons and holes inside the particles. Because the photoinduced electrons and holes can be incorporated into redox reactions on the titania surface before spontaneous recombination, the surface states of the titania particle are quite important for photoreactivity [37-52].

Titania has three polymorphs: anatase, rutile, and brookite. Anatase thin film deposition on a glass substrate has been achieved using the MPM. A water-resistant coating solution was prepared by the reaction of a neutral  $[\text{Ti}(\text{H}_2\text{O})(\text{EDTA})]$  complex (EDTA is ethylenediamine-*N,N,N',N'*-tetraacetic acid) with dipropylamine in ethanol [1, 2, 4-9]. The anatase phase appears during the heat-treatment of the precursor film at a temperature between 400 and 500°C and is transformed to the rutile one between 500 and 700°C. X-ray diffraction (XRD) analysis of the films prepared by a conventional sol–gel process showed that the anatase phase appeared between 400 and 500°C and was not transformed to the rutile one, even when heat-treated at 900°C. The irreversible phase transformation from anatase to rutile requires heat-treatment. During heat-treatment of anatase, the atoms in the original tetragonal lattice can be rearranged into the rutile tetragonal lattice. The temperature difference between the phase transformation from anatase to rutile in the sol–gel method and the MPM will be discussed in the section **O deficiency in rutile thin films**.

## 5. Vis-responsive anatase thin film fabricated using the MPM

Many researchers study the fabrication and photoreactivity of Vis-responsive thin films by physical and/or chemical modification of anatase films because of the importance of Vis-photoreactive materials [53-61]. However, there is little information on the enhancement of UV sensitivity of Vis-responsive anatase films.

The implantation of various transition-metal ions such as  $\text{V}^{5+}$ ,  $\text{Cr}^{3+}$ , and  $\text{Cu}^{2+}$  into the lattice of  $\text{Ti}^{4+}$  in anatase thin films was investigated by Anpo *et al.* [62-67]. The photoreactivities of chemically modified anatase thin films decreased under UV irradiation, although those anatase thin films modified with transition-metal ions can behave as photocatalysts under Vis irradiation. Since Asahi *et al.* reported that non-metallic ions such as a substitutional nitride ion at the oxygen sites of anatase are also effective at enabling the thin film to be responsive to Vis light, methods for modifying anatase with tetravalent carbon or hexavalent sulfur cations have also been investigated [68]. Miyauchi *et al.* achieved another chemical fabrication of Vis-responsive anatase thin films, which were modified under  $\text{NH}_3$  gas by heat-treating the resulting films formed using a sol–gel method [69]. However, the photoreactivities of those films are lower under UV irradiation than those before modification in all cases. Nevertheless, they can work as photocatalysts under Vis light. Thus, studies on the chemical formation of Vis-responsive anatase thin films with enhanced

photoreactivities under UV irradiation are significant from the viewpoint of solar energy efficiency.

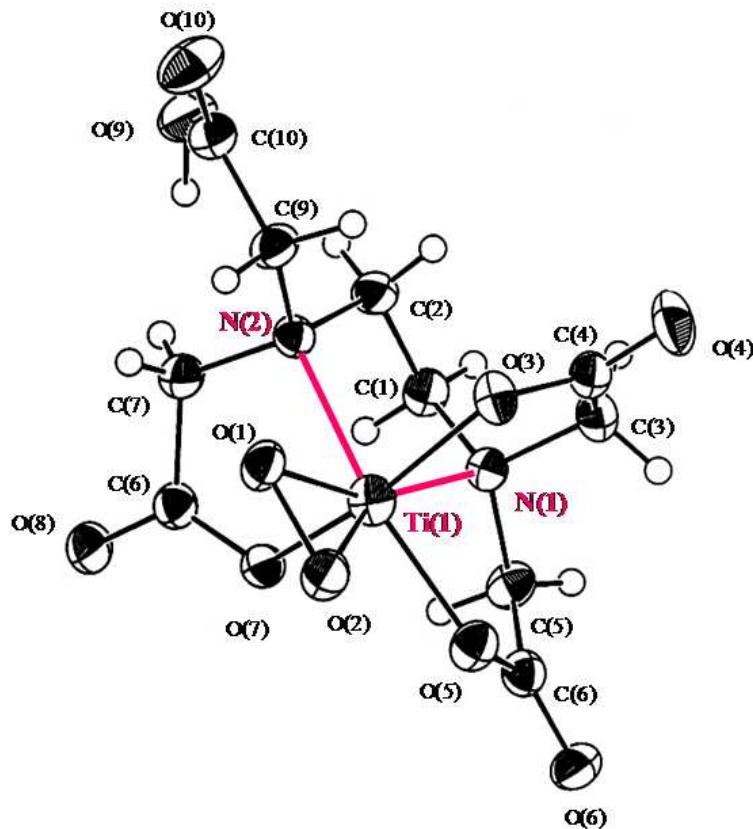


**Figure 3.** An ORTEP view of the precursor complex having the EDTA and peroxo ligands linked to the central  $Ti^{4+}$  ion. The molecular structure was determined by an X-ray single crystal structure analysis of the diethylammonium salt of the complex, although the dibutylammonium salt was employed for the coating solution in order to prevent from the crystallization of the precursor. The single crystals of the identical orange-yellow color could be obtained from a reacted solution of the complex with the diethylamine instead of dibutylamine. The single crystal was  $\{(C_2H_5)_2NH_2\}[Ti(O_2)(Hedta)] \cdot 1.5H_2O$ ; in a monoclinic crystal system,  $P2_1/c$  with  $a = 8.583(1)$ ,  $b = 6.886(1)$ ,  $c = 36.117(2)$  Å, and  $\beta = 92.780(3)^\circ$ . The full-matrix least-squares refinement on  $F^2$  was based on 3206 observed reflections that were measured at 250 K by using an imaging plate as a detector, and converged with unweighted and weighted agreement factors of  $R = 0.054$  and  $R_w = 0.061$  respectively, and  $GOF = 1.63$ . Two Ti–N(edta) bond lengths of 2.307 and 2.285 Å, are slightly longer than the bond length of 2.12 Å in the TiN single crystal. Results indicated that EDTA acts as a pentadentate ligand in the complex, and the peroxo ligand linked to the  $Ti^{4+}$  ion has a side-on coordination structure.

The MPM forms transparent titania thin films using the ethanol solution obtained as a coating solution ( $S_{ED}$ ) by the reaction of alkylamine with a titanium complex of EDTA as the ligand [1, 2, 4-9]. According to single-crystal structural analysis, this Ti complex contains Ti–N bonds (Figure 3). If the Ti–N bonds in this complex can be preserved in the anatase thin film obtained by heat-treatment after coating, a partially nitrated anatase film can be directly formed. However, XRD and X-ray photoelectron spectroscopy (XPS) confirmed that the precursor film formed on a glass substrate using the ethanol solution is transformed into

a nitrogen-free anatase thin film through heat-treatment for 30 min in air at a temperature of 450°C or higher. Based on these results, the heat-treatment of molecular precursor films spin-coated with SED on ITO glass substrates was examined in an Ar gas flow of 0.1 L min<sup>-1</sup> at 500°C for 30 min. The XRD pattern indicated that the spin-coated precursor film crystallized to anatase through heat-treatment at a temperature of 500°C or higher under atmospheric conditions. Thus, the anatase form was created even if oxygen was not supplied externally to remove organic residues in the metal complex. Furthermore, the chemical bond toward the Ti<sup>4+</sup> ion from both oxygen and nitrogen atoms can be observed in the XPS spectra of the resultant thin films. The binding energies of Ti 2p<sub>3/2</sub> attributed to Ti–O and Ti–N had typical values of 459.1 and 455.3 eV, respectively (Figure 4) [5, 70-72]. Importantly, the binding energy of N 1s was 396.7 eV, and the existing nitrogen was only in the oxygen-substituted form, not in the chemisorbed form [73, 74]. Thus, the heat-treatment of the precursor films in an Ar gas flow was effective in preserving nitrogen atoms in the complex. However, the photoreactivity of the thin film was not observed after Vis irradiation with a weak fluorescent lamp. Because the partially nitrated film obtained by the MPM alone did not respond to irradiation with a fluorescent lamp, a precursor solution, Sox, with no Ti–N bonds, in complexes whose ligand was oxalic acid (OX), was freshly prepared and the layering of the anatase films was achieved using the two precursor solutions.

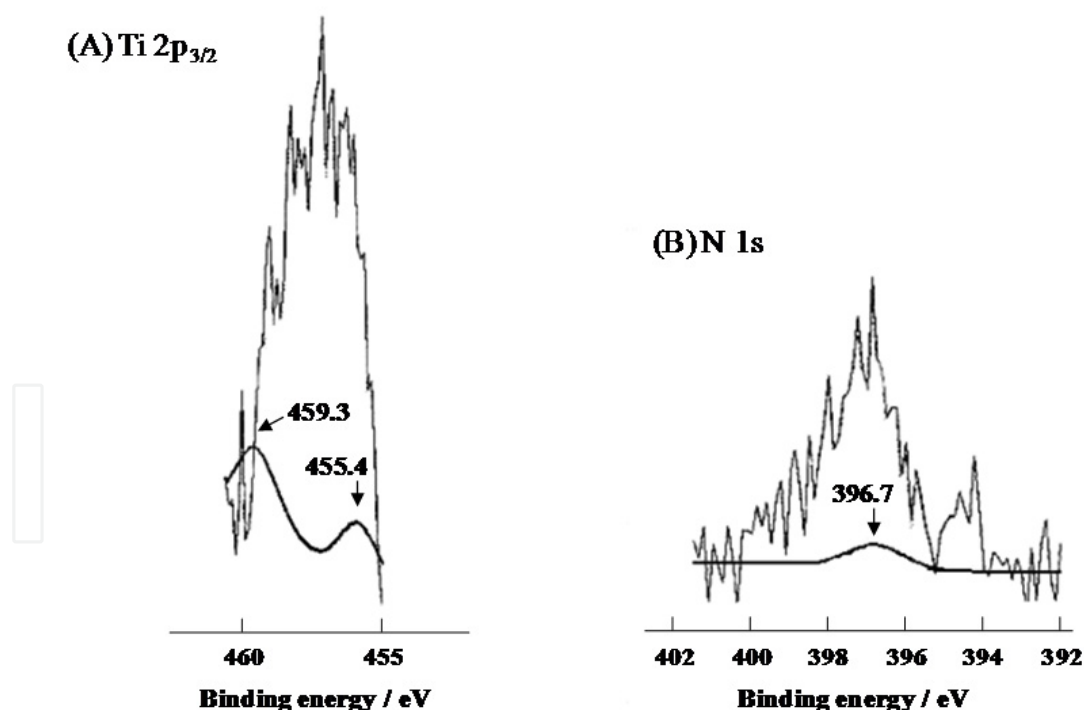


**Figure 4.** XPS spectra of (A) Ti 2p<sub>3/2</sub> and (B) N 1s of the nitrogen-substituted TiO<sub>2</sub> thin film obtained by heat treatment of the precursor film containing the Ti complex with EDTA ligand on a Na-free glass in an Ar gas flow. The thin solid lines are original data of XPS. The thick solid curves are theoretical Gaussian distribution curves. The dashed curves are theoretically fitted curves by assuming Gaussian distribution [5].

Two types of three-layer film, **OX–OX–OX** and **OX–ED–OX**, were formed on an ITO pre-coated glass substrate by coating and heat-treating the precursor films under an Ar gas flow. A schematic diagram of these structures is shown in Figure 5. The first layer, of thickness 100 nm, was formed by applying Sox. The second and third layers were 50 nm thick. The third layer of **OX–OX–OX** was fabricated as a reference by applying only Sox, although the corresponding layer of **OX–ED–OX** was fabricated on the second layer using  $S_{ED}$ , and then the third layer was formed with Sox (Figure 6). The overall amount of the heat-treated molecular precursor, energy consumed, film area, and film thickness were kept constant.

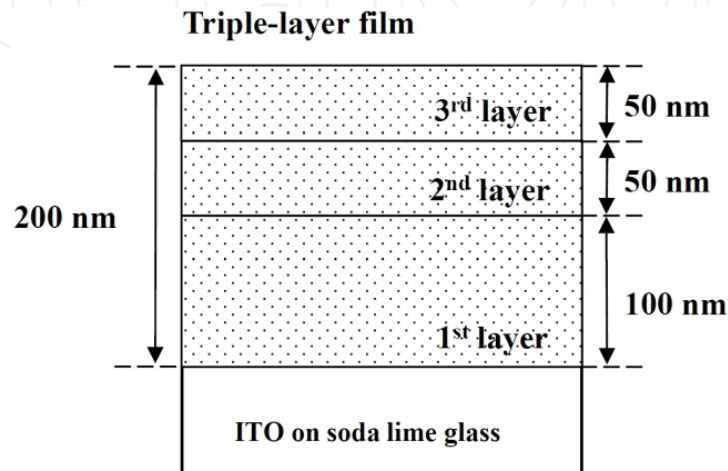


**Figure 5.** Schematic diagram structures of triple layer thin films. Each precursor film for the first layers was formed by applying Sox and heat-treated at 475°C for 30 min. The precursor film of the second layer for **OX–OX–OX** formed by employing the half-diluted solution of Sox, and **OX–ED–OX** formed by using the half-diluted solution of  $S_{ED}$  were heat-treated at 500°C for 30 min. The precursor films of the third layers for **OX–OX–OX** and **OX–ED–OX** formed by employing the half-diluted solution of Sox were heat-treated at 475°C for 30 min.

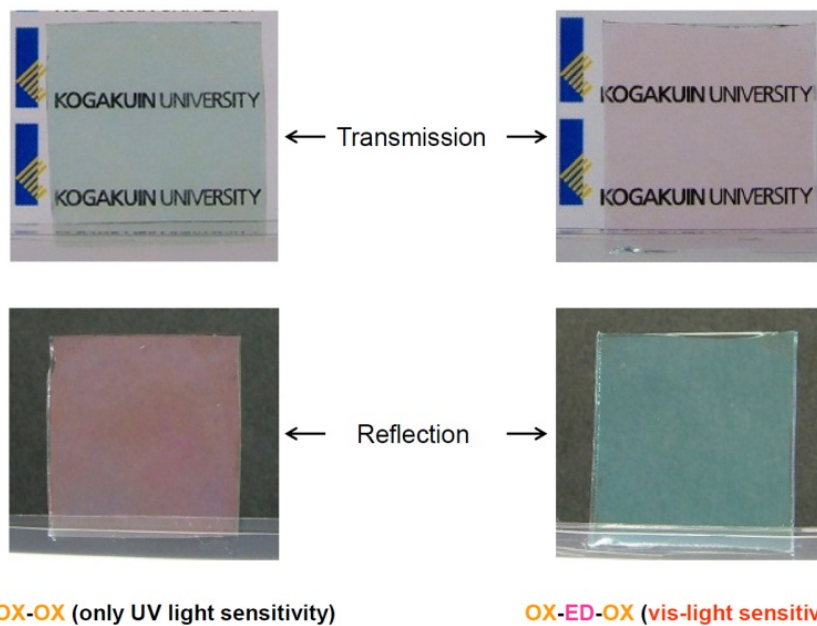


**Figure 6.** Photographs of the 3-layer **OX–OX–OX** and **OX–ED–OX** films on the ITO glass substrate.

The XRD patterns of both films indicated that anatase was formed. The field-emission scanning electron microscopy (FE-SEM) data of both films show even surfaces without cracks or pinholes. These surfaces were too smooth to detect the roughness by measuring with a stylus profilometer, whose detective limit is ca. 10 nm. The XPS depth profiles of these films are shown in Figure 7. The depth profile for **OX-ED-OX** revealed that nitrogen and carbon were locally distributed in the deep portion corresponding to the second layer. A relative decrease in the amount of oxide ions in the corresponding layers was observed. This suggests that other anions, *e.g.*, nitride ions, compensate for the charge balance. This confirmed that significant amounts of carbon and nitrogen atoms were still present in the second layer, and the substitutional nitrogen atoms were locally distributed in the deep portion corresponding to the second layer. Most nitrogen atoms did not diffuse to other layers, although the amounts of nitrogen and carbon atoms in the other layers could not be neglected. The absorption spectra of **OX-ED-OX** indicate characteristic absorption bands near 480 nm. The **OX-OX-OX** films do not show such absorption bands in the Vis-light region.

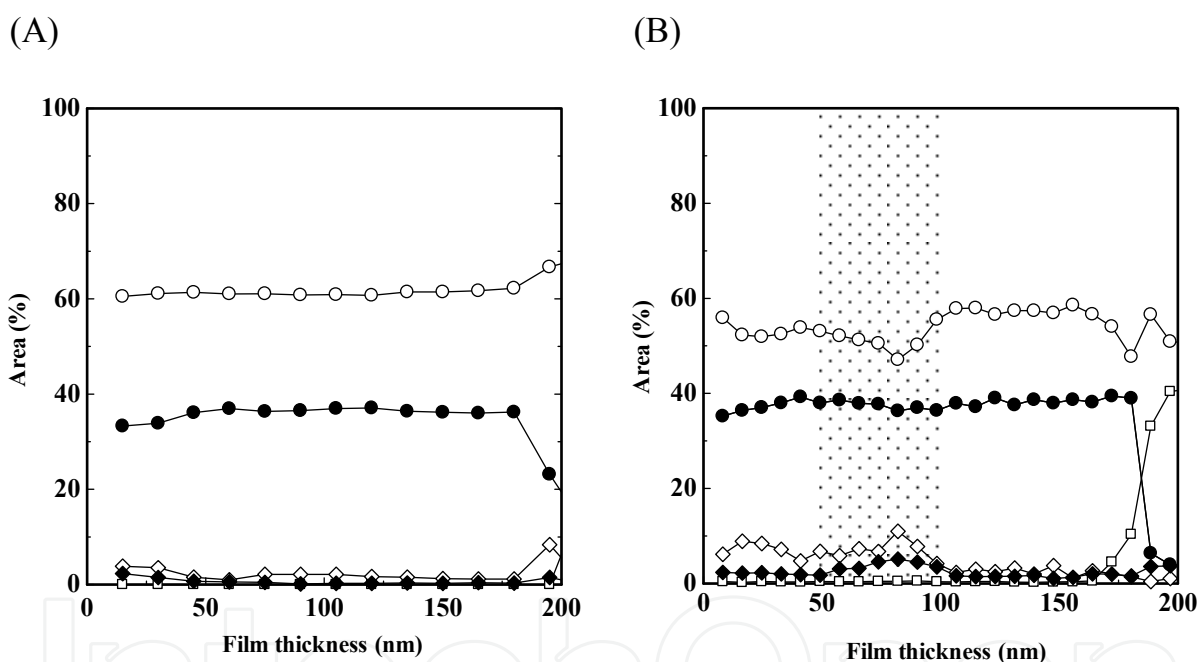


**Figure 7.** Depth profile of the amount of components in the 3-layer thin film (A) **OX-OX-OX** and (B) **OX-ED-OX**. Notations indicate the energy levels of five atoms in parentheses, —●— (Ti 2p), —○— (O 1s), —◆— (N 1s), —◇— (C 1s), —□— (In 3d). Net multiplication part is corresponding to the second layer formed by applying the solution **S<sub>ED</sub>**.

The photoreactivities of the films were tested using the decolorizing reaction of methylene blue (MB) aqueous solution [5-8, 75-77]. The decoloration rate of 0.01 mol L<sup>-1</sup> MB solution by the photoreaction with both multilayered thin films under UV or Vis irradiation are summarized in Table 1. The **OX-ED-OX** film has an effective photoreactivity under Vis irradiation. The **OX-OX-OX** film only responded to UV light. It is important that the photoreactivities of the Vis-responsive films are also extremely high under UV irradiation.

The Vis-responsive property of the **OX-ED-OX** film was mainly due to the colored materials that were formed spontaneously during heat-treatment by chemical reactions between the reductant derived from the precursor complex containing OX in the upper layer and the organic residues derived from EDTA ligands in the lower one. Thus, the thermal reactions between the residues derived from the ligand of the precursor complex can afford novel functions such as the Vis-responsive nature of the resultant thin films through heat-treatment of the thin films fabricated by the MPM. The design of metal complexes for the precursor and of the heating program are crucial.

Multilayer film	$\nu$ [nmol L <sup>-1</sup> min <sup>-1</sup> ]	
	under UV irradiation	under VIS irradiation
<b>OX-OX-OX</b>	16(1)	—
<b>OX-ED-OX</b>	21(1)	6(1)

**Table 1.** The rate  $\nu$  [nmol L<sup>-1</sup> min<sup>-1</sup>] of decoloration rate of 0.01 mol L<sup>-1</sup> MB solution by the photoreaction with both thin films under UV and VIS irradiation [5]. The rate was measured by the decrease of absorption value at 664 nm of each test solution. Those obtained from the data measured under dark are also indicated. Calculated standard deviations are presented in parentheses.

## 6. Formation of O-deficient anatase thin film

To clarify the factors for designing an anatase thin film with a higher photoreactivity under UV irradiation, the relationship between the photoreactivity and O deficiency of anatase thin films fabricated with the heat-treated precursor films under regulated conditions was examined. Thin films were formed by heat-treating precursor films spin-coated onto FTO glass substrates with **S<sub>ED</sub>** and **S<sub>SG</sub>** (sol-gel solution) under Ar or air.

The spin-coating method at ambient temperature was used for forming precursor films using a double-step method. The first step used 500 rpm for 5 s and the next step was 2000 rpm for 30 s, in all cases. The precursor films were pre-heated in a drying oven at 70 °C for 10 min and then heat-treated at 500°C for 30 min in a 0.1 L min<sup>-1</sup> Ar gas flow. A tubular furnace made of quartz was employed for the heat-treatment. Thin films, **ED** and **SG**, were formed by applying the precursor solutions **S<sub>ED</sub>** and **S<sub>SG</sub>**, respectively, before annealing in air. The film **ED<sub>air</sub>** was fabricated by firing the precursor film spin-coated with **S<sub>ED</sub>** in air at 500°C for 30 min.

When the concentration of titanium was 0.4 mmol g<sup>-1</sup> for **S<sub>ED</sub>**, the film thickness was 100 nm. An **S<sub>SG</sub>** of 0.5 mmol g<sup>-1</sup> was stirred for 3 days at ambient temperature to fabricate an anatase film of thickness 100 nm. The post-annealing treatment for the **ED**, **ED<sub>air</sub>**, and **SG** thin films was carried out in air at 500°C for 5, 10, 15, 20, and 30 min. The number in the notation used for post-annealed films indicates the annealing time (min). For example, **ED-PA5** indicates an **ED** film post-annealed for 5 min. The photoreactivities of the thin films are presented in Table 2. Each value was calculated as the difference between the decoloration rate under UV-light irradiation and the corresponding value measured for each thin film in the dark.

The maximum photoreactivity of **ED-PA15** produced by the MPM is twice that of **SG-PA10** prepared by a conventional sol–gel procedure.

Annealing Time (min)	$\nu$ under UV-light irradiation		
	<b>ED</b>	<b>ED<sub>air</sub></b>	<b>SG</b>
0	2(1)	6(1)	5(1)
5	5(1)	12(1)	6(1)
10	9(1)	12(1)	8(1)
15	16(1)	9(1)	7(1)
20	11(1)	9(1)	7(1)
30	8(1)	5(2)	5(1)

**Table 2.** The rate  $\nu$  [ $\text{nmol L}^{-1} \text{min}^{-1}$ ] of decoloration rate of  $0.01 \text{ mol L}^{-1}$  MB solution by the photoreaction with each thin film under UV-light irradiation [6]. The rate was measured by the decrease of absorption value at 664 nm of each test solution. Those obtained from the data measured under dark are also indicated. Calculated standard deviations are presented in parentheses.

It is generally accepted that the main factors to consider when designing enhanced photoreactivity of anatase are (1) higher crystallinity, (2) larger surface area, and (3) decreased impurities. The crystallite size is an indicator of crystallinity [78, 79]. Among the crystallite sizes of the three anatase thin films, **ED**, **ED<sub>air</sub>** and **SG**, the **SG** thin film had the largest value and the **ED** film had the smallest (Table 3). These values for the anatase crystallites in **ED<sub>air</sub>** and **SG** thin films were not affected by post-annealing treatment in air. The thin film **ED-PA15** (whose crystallite size was the smallest) showed the highest photoreactivity in the decoloration of an MB aqueous solution among the various thin films formed in this study. The specific surface areas of the thin films were not measured quantitatively because of the difficulties involved. However, the degrees of adsorption of MB molecules in aqueous solution were nearly equal among the thin films, including those formed by the sol–gel method. Therefore, the differences in the photoreactivity among these thin films should be due to other factors than the specific surface area. The XPS spectra suggested that the thin films **SG** and **SG-PA $n$**  have higher purities than the other thin films. Therefore, the highest photoreactivity, of **ED-PA15** thin film, cannot be due to its purity. The O/Ti peak area ratio determined from the XPS of the anatase film **ED-PA15** with the highest photoreactivity was extremely small, 1.5. The refractive indices of the thin films **ED<sub>air</sub>** and **SG** increased gradually, depending on the post-annealing time. On the other hand, the refractive index of the **ED** thin film decreased with post-annealing treatment time up to 15 min and then increased with further annealing. The largest index (2.17; **ED** thin film) may be related to the strong and wide absorbance by the above-mentioned impurities. Furthermore, the smallest value (1.99; **ED-PA15**) could be affected by the largest O deficiency in the anatase thin film after purification. The decrease in permittivity of the thin film arose from the lower charge density derived from the O deficiency because the structure of the anatase lattice is rigid. Thus, the O deficiency formed by this method was one of the most important factors for fabricating highly UV-sensitive anatase. This O deficiency was formed during heat-treatment of the precursor metal complexes.

A coordination skeleton of  $(\text{TiO}_4\text{N}_2)$  or  $(\text{TiO}_5\text{N}_2)$  can be assumed in the EDTA complex as a precursor molecule from the structural study of a Ti complex  $[\text{Ti}(\text{H}_2\text{O})(\text{EDTA})] \cdot 1.5\text{H}_2\text{O}$  reported by Fackler *et al.* [80]. In the precursor films, two N and at least four O atoms link to one Ti ion. As a result of heat-treating the precursor complex in an Ar gas flow, neighboring complexes reacted with each other. In this process, several O atoms linked to one Ti ion could be covalently bonded by other Ti ions, and the anatase lattice was gradually created. By eliminating large amounts of C, H, and N atoms with O atoms, oxide ion sites of the anatase lattice were partially occupied by a rather stable nitride ion derived from the coordinated N atom originally belonging to the ligand. As a result, the total negative charge of the N-substituted anatase in the **ED** thin film is ca. 3.6 toward one Ti ion. This value is the summation of 2.8 from the oxide ions and 0.8 from the nitride ions. This charge toward one Ti ion is larger than that of ca. 3.3 by the oxide ions in the **SG** thin film. The substitutional N atoms could be removed from the anatase lattice by post-annealing the **ED** thin film. Consequently, the total negative charge of the **ED-PA15** thin film, whose photoreactivity is the highest, decreased to ca. 3.0. Longer annealing treatment replenished oxide ions in the anatase thin films from their surfaces and the photoreactivity decreased (Figure 8) [6]. Thus, it was elucidated that O deficiency is an important factor to consider when designing anatase photoreactivity. It is also notable that the O-deficient anatase lattice is rather robust because the stoichiometric  $\text{Ti}_2\text{O}_3$  did not appear at all.

Annealing Time (min)	Crystallite size (nm)		
	ED	ED <sub>air</sub>	SG
0	—	10	13
5	—	10	13
10	5	11	13
15	4	10	13
20	7	11	13
30	7	12	13

**Table 3.** The crystallite size of anatase in **ED**, **ED<sub>air</sub>**, **SG** and post-annealed thin films [6]. The crystallite size of anatase was measured with a typical Scherrer-Hall method by employing a peak assignable to only (1 0 1) of anatase, because other peak intensities due to anatase were too low to measure accurately. The crystallite size of anatase in **ED** and **ED-PA5** could not be obtained because the (1 0 1) peak of anatase was also too weak to determine the crystallite size.

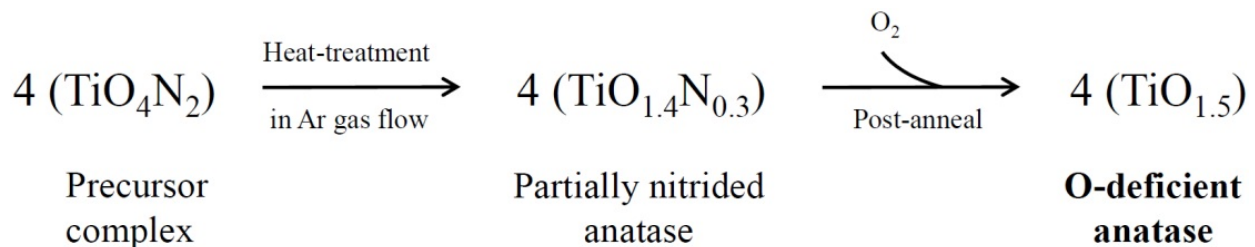


**Figure 8.** Plausible route of the O-deficient anatase lattice formation from the precursor complex skeleton through the heat treatment in an Ar gas flow and the sequential post-anneal [6].

## 7. O deficiency in rutile thin film

Rutile is the most stable crystal form of titania. Since Nishimoto *et al.* showed that anatase is more sensitive to UV light than rutile in photoreactions, rutile was believed to be inferior to anatase in terms of photoreactivity [81]. Anatase is important for photocatalysis in pollutant degradation and in the development of photofunctional materials such as films with hydrophilic surfaces under UV-light irradiation. The poor photoreactivity and photosensitivity of rutile is generally believed to be due to its crystal structure. Rutile is primarily known as a useful pigment for white paint, due to its chemical stability [82, 83].

Because the band edge of a rutile single-crystal is 3.0 eV, rutile has the potential to respond to Vis light. Using this knowledge and the results of previous experiments on anatase responses to Vis light, this section describes an attempt to achieve direct fabrication of O-deficient rutile thin films with high photoreactivity using a MPM. The first Vis-light-responsive thin film created from O-deficient rutile is discussed here. This material works without application of an electric potential, due to its unprecedentedly high photosensitivity under UV-light irradiation. The present findings should facilitate widespread practical use of rutile in light-related applications.

The thin films were formed by heat-treating the precursor films after spin-coating onto a quartz glass substrate.  $S_{ED}$  and  $S_{SG}$  were applied in an Ar gas flow. The transparent precursor films formed by spin-coating the solutions and pre-heating in a drying oven at 70 °C for 10 min were heat-treated at 700 °C for 30 min in a furnace made from a quartz tube with an Ar gas flow rate of 0.1 L min<sup>-1</sup>. When  $S_{ED}$  was used, a transparent rutile thin film **R** was formed. When  $S_{SG}$  was used, a transparent anatase thin film **A** was formed. The film thickness was 100 nm in both cases.

Each structure was characterized using XRD, Raman spectroscopy, and transmission electron microscopy (TEM). The selectivity was due to the O-vacant sites in the oxide thin films formed at different levels due to the differences between the amounts of oxygen in the two precursors. In this case, the oxygen source required to structure titania was available only in the precursor films when these thin films were fabricated. Therefore, crystallization into rutile, which has many O-vacant sites, and the accompanying rapid elimination of organic residues from the **R** precursor film, occurred because of the heat-treatment.

In contrast, the amount of oxygen available to Ti<sup>4+</sup> in titanoxane polymers, though significant, was insufficient to develop stoichiometric TiO<sub>2</sub> from **A**. The oxygen defects in an anatase lattice generally lower the temperature of the phase transformation from anatase to rutile [84, 85]. Thus, selective formation occurred according to the differing degrees of O deficiency.

The photoreactivities of the thin films were evaluated by the decoloration rates of MB solutions, which served as a model for organic pollutants in water. The results measured under Vis- and UV-light irradiation are summarized in Table 4, along with those measured under dark conditions (reference values). The data show the effects of adsorption on the samples, vessels, and self-decoloration of MB under each condition. Moreover, the

photoreactivity of **R** was extremely high under UV irradiation and higher than the photoreactivity of **A**. This is without precedent.

Notation	$\nu$ [nmol L <sup>-1</sup> min <sup>-1</sup> ]	
	under visible light	under UV light
<b>R</b>	9(1)	23(1)
<b>A</b>	–	15(1)

**Table 4.** The reaction rate  $\nu$  of the decoloration reaction in an aqueous solution containing 0.01 mol L<sup>-1</sup> of methylene blue under visible- and UV-light irradiation and under dark conditions [7]. Calculated standard deviations are presented in parentheses.

The photosensitivities of **R** and **A** were also examined by measuring the effects of Vis and UV irradiation on the water contact angle for the surfaces of the thin films. The results are shown in Figure 9 [7]. The rutile thin film **R** exhibited Vis-light-induced hydrophilicity with a fluorescent light, even though high-energy light below 400 nm was eliminated. In contrast, Vis light alone did not reduce the contact angle on **A** under the same conditions. Furthermore, a rapid decrease in the water contact angle for **R** was observed with weak UV-light irradiation. The super-hydrophilic property of **R** appeared after only 1 h. When fluorescent light with a UV component was employed, the contact angle on **R** rapidly reduced and the values reached 38° and 10° after irradiation for 1 and 24 h respectively.

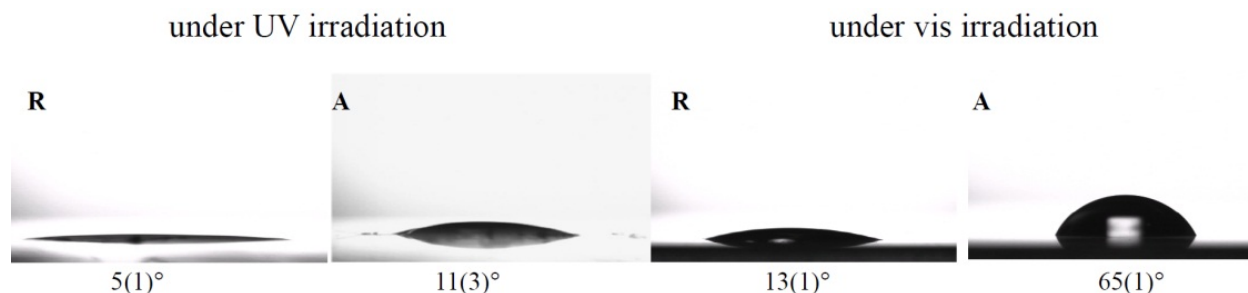


**Figure 9.** Comparison of the contact angles of a 1.0- $\mu$ L water droplet on the thin films **R** and **A**. Before the measurement, the thin films were exposed to UV irradiation of 1.3 mW cm<sup>-2</sup> at 356 nm obtained by a black light (each on the left side), and to visible light without UV light was obtained from a fluorescent light by removing light of wavelengths shorter than 400 nm using a cut-off filter. The Vis light intensity after removing UV components from the fluorescent light, which was estimated by an illuminometer was 0.8 mW cm<sup>-2</sup> [7].

It is noteworthy that the simple fabrication of a Vis-responsive rutile film with high photoreactivity could be attained. Thus, the O defects in titania are also effective at providing photoreactivity of rutile, which is usually insensitive to both UV and Vis light.

## 8. Crystal orientation and photoluminescence of rutile in thin film

PL emission has been widely used to investigate the efficiency of charge carrier trapping, migration, and transfer, and to understand the fate of electron-hole pairs in semiconductor particles [86]. It is therefore helpful to examine the position and intensity of the PL bands of

semiconductor particles to understand the photoreactivities of the particles [87]. In this section, we report the changes in the PL and photoreactive properties of the Vis-responsive rutile thin film fabricated by the MPM, which are effected by annealing in air at 700°C. The relationship between O deficiency and PL emission was examined to understand the incredibly high photoreactivity of the rutile thin film. Furthermore, the level of crystal orientation of the rutile thin film was quantitatively evaluated on the basis of data from XRD analyses. The amount of oxygen supplied during the annealing process was analyzed by XPS measurements. The growth of crystals and particles was also investigated by crystallite-size measurements and SEM observations. The heat-treatment of the fabricated O-deficient rutile **R** thin film was carried out in air at 700°C for 15, 30, and 60 min. The number in the notation of the post-annealed films indicates the annealing time (min). For example, **R-PA15** indicates that post-annealing treatment of the **R** thin film was carried out for 15 min. The extent orientation factor ( $f$ ) for the (110) plane of the **R-PA $n$**  thin films increased with annealing time in air (Table 5).

Film	Crystallite size <sup>a)</sup> / nm	Orientation factor; $f$	O/Ti ratios	
			Surface	Deeper portion
<b>R</b>	15(2)	0.35	1.74	1.75
<b>R-PA15</b>	21(3)	0.67	1.84	1.73
<b>R-PA30</b>	21(3)	0.69	1.89	1.79
<b>R-PA60</b>	20(4)	0.75	1.94	1.85

**Table 5.** The crystallite size, orientation factor and O/Ti ratio of rutile crystals in the **R** thin film and in the post-annealed **R-PA $n$**  thin films [8]. The crystallite size of rutile was measured with a typical Scherrer-Hall method by employing the peaks assignable to (1 1 0), (1 0 1) and (2 1 1) of rutile. The extent of the orientation was estimated in terms of Lotgering orientation factor,  $f$ , from the XRD peak intensities ( $I$ ). For calculating the orientation factor, the intensity data of non-oriented rutile was cited from the JCPDS card 21-1276. The O/Ti ratios determined by the XPS peak areas of O 1s and Ti 2p<sub>3/2</sub> peaks observed from the surfaces of **R** and post-annealed thin films. The XPS peaks of the thin film surface were measured without bombarding Ar<sup>+</sup> ion beam. The peak area of O 1s and Ti 2p was calculated by FWHM and peak height at the positions 531.0 and 459.0 eV, respectively. The averaged O/Ti ratios determined by the XPS peak areas of O 1s and Ti 2p<sub>3/2</sub> peaks of **R** and post-annealed thin films. The XPS peaks of thin films were measured after bombarding Ar<sup>+</sup> ion beam with 2 kV and 18  $\mu\text{A cm}^{-2}$  for 3 min, in order to remove surface oxides. The peak area of O 1s and Ti 2p was calculated by FWHM and peak height at the positions 531.0 and 459.0 eV, respectively, obtained from each depth profile in Ar<sup>+</sup> ion etching mode.

a) The estimated standard deviations are presented in parentheses

The extent orientation could be estimated from the XRD peak intensity by using the Lotgering method [8]. The terms  $I(hkl)_{\text{ideal}}$  and  $\Sigma I(hkl)_{\text{ideal}}$  are defined as the intensity of the peak attributable to the specific plane ( $hkl$ ) and the sum of each intensity obtained for the non-oriented rutile crystals; thus,  $P_0$  can then be expressed as

$$P_0 = I(hkl)_{\text{ideal}} / \Sigma I(hkl)_{\text{ideal}} \quad (1)$$

In this study, each  $I(hkl)_{\text{ideal}}$  value was cited from the standard data of the corresponding rutile phase.

The definitions of the terms  $I(hkl)_{\text{obsd}}$  and  $\Sigma I(hkl)_{\text{obsd}}$  for the thin films **R** and **R-PAn** are identical to those for  $\Sigma I(hkl)_{\text{ideal}}$  and  $I(hkl)_{\text{ideal}}$  in equation (1), respectively, and the  $P_n$  value can be calculated as

$$P_n = I(hkl)_{\text{obsd}}/\Sigma I(hkl)_{\text{obsd}} \quad (2)$$

The Lotgering orientation factor  $f$  is defined as

$$f = (P_n - P_0)/(1 - P_0) \quad (3)$$

The factor  $f$  is defined for  $P$  or  $P_0$  values over a certain range of  $2\theta$ . As the level of orientation increases, the  $f$  value will increase from 0 to 1. The factor  $f$  is therefore a measure of the crystal phase orientation. Consequently, the  $f$  value of the **R** thin film was the smallest among the thin films fabricated by the MPM. However, the present  $f$  value of the **R** thin film was larger than those reported for rutile thin films fabricated by a sol-gel method on several substrates such as quartz glass, alumina, and single-crystals of quartz or silicon [88]. This result may be related to the different mechanisms governing the formation of the rutile lattice. In the sol-gel method, the  $\text{Ti}^{4+}$  and  $\text{O}^{2-}$  ions that are tightly linked in titanoxane polymers formed by the condensation of partially hydrolyzed alkoxide might be rearranged to form the rutile lattice at a higher temperature. In the MPM, however, small units composed of  $\text{Ti}^{4+}$  and  $\text{O}^{2-}$  ions with higher mobility could be formed when the organics were decomposed and removed by heat-treating the precursor complex. Therefore, a rutile thin film with a higher level of crystal orientation could be formed at these lower temperatures.

After 15 min of heat-treatment in air, the crystallite size of the **R** thin film increased, while those of the **R-PAn** thin films remained almost constant (Table 5). These results indicate that crystallite growth at a temperature of  $700^\circ\text{C}$  was completed by heat-treatment over a period of 30–45 min. The additional thermal energy was consumed mainly for the process of grain growth after crystallite growth because the grain size gradually increased with annealing time.

Previously, the peak position of the PL emission band obtained for rutile crystals was observed at ca. 450 nm [89]. However, PL emission bands of the **R** and **R-PAn** thin films formed by the MPM were not detected at 450 nm (Figure 10) [8].

Nakamura *et al.* reported that in the case of a rutile single-crystal, the PL emission band attributable to the (110) plane can be observed at 810 nm [90]. Taking into account the high levels of crystal orientation with reference to the (110) plane in the **R** and **R-PAn** thin films, the PL emission bands observed at around 800 nm in the spectra of the **R-PAn** thin films can be attributed to rutile crystals oriented along the (110) plane in these thin films (Figure 11) [8].

For the O-deficient rutile thin film **R** with high photoreactivity, no PL emission was observed in the range 190–850 nm. Thus, as previously suggested, the O-defect sites on the rutile thin film may suppress recombination of the photoinduced electron-hole pairs by electron trapping. In contrast, the PL emission from rutile thin films after annealing in air may be due to the oxide ions that are supplied to the O-defect sites on the film surface, because they function as recombination centers. As a result, the lattice oxygens of titania, especially in rutile thin films, function as recombination centers for the photoinduced electron-hole pairs.

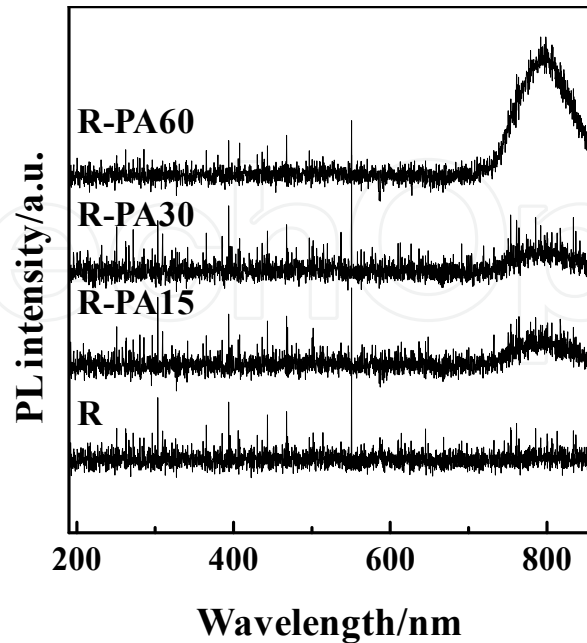


**Figure 10.** The photoluminescence emission spectra of the thin films, O-deficient rutile **R** and post annealed **R-PA $n$**  ( $n = 15, 30, 60$ ). The spectra were measured in the wavelength range 190-850 nm at room temperature [8].

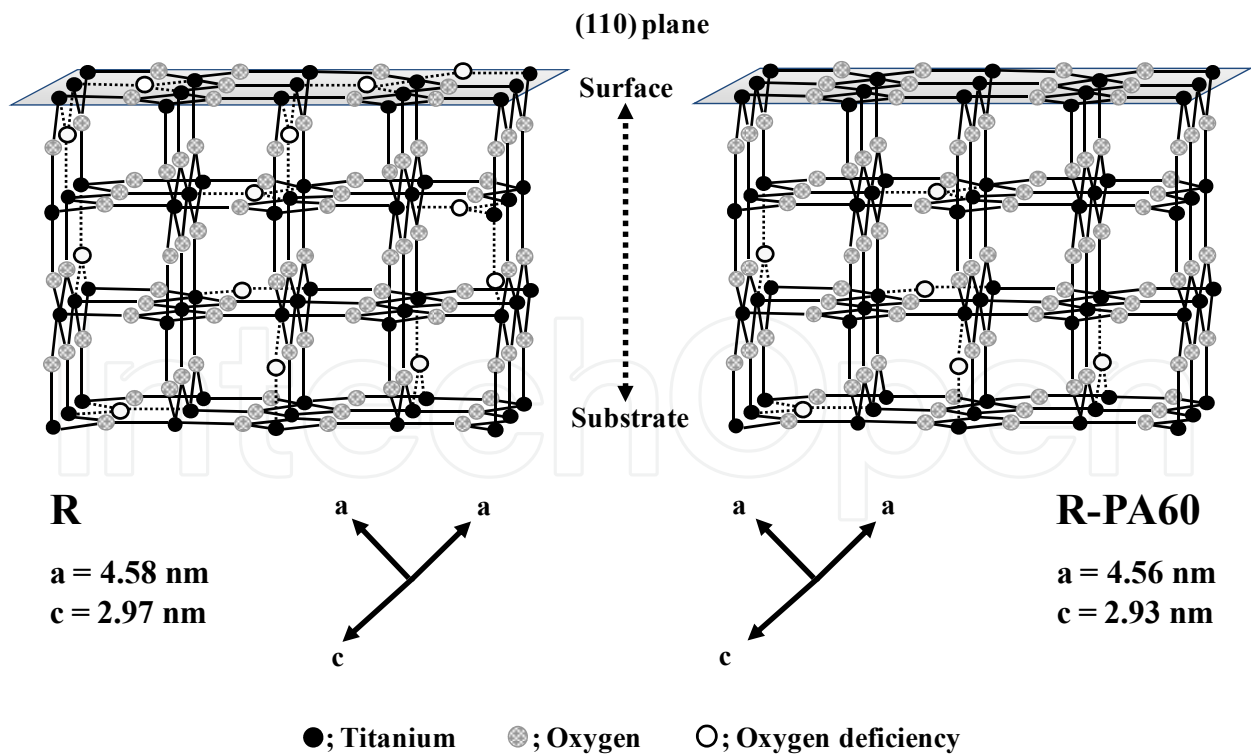


**Figure 11.** Proposed schematic diagrams for the (110) plane orientated O-deficient rutile **R** (left) and post annealed **R-PA60** (right) thin films are shown. Cell parameters were refined by a least square method [8].

The reduction of rutile surfaces by heated hydrogen activates the photoreactivities of these surfaces [36]. As a result, the formation of an oxygen deficiency provides photoreactivity. The present study revealed that the unprecedentedly high photoreactivity of the **R** thin film is suppressed by oxygen supply during the annealing process. However, the high levels of photoreactivity of these films could be maintained even after oxygen supply to the surface by the post-annealing treatment (Table 5). These results indicate that the enhanced photoreactivity is related not only to the surface but also to the inner part of the thin films as a result of an interparticle electron transfer (IPET) effect, as proposed in our previous paper.

## 9. Highly conductive Ag-nanoparticle/titania composite thin films

An excellent perovskite-type  $\text{SrTiO}_3$  thin film was fabricated using a mixed precursor solution from a titania precursor solution containing a Ti complex of EDTA and an SrO precursor solution containing a Sr complex of EDTA [4]. The metal complex ions dissolve independently in each precursor solution and the homogeneity of the mixed solution can be kept at the molecular level. In fact, a mixed precursor solution containing exact amounts of Ti and Sr can be easily prepared due to the excellent miscibility of the solutions. This is the essential difference between the MPM and conventional sol–gel methods in which the hydrolyzed polymers are heterogeneous because of the different rates of hydrolysis of each metal ion. On the basis of this excellent miscibility in the MPM, Ag-nanoparticle/titania (Ag-NP/ $\text{TiO}_2$ ) composite thin films with a wide range of volumetric fractions of Ag in the titania matrix were developed using the titania precursor  $\text{S}_{\text{ED}}$  [9].

Many researchers have tried to incorporate metal nanoparticles into semiconductor materials to improve the conductivity of the semiconductor. The  $\text{TiO}_2$  film's relatively high resistivity of  $10^{12} \Omega \text{ cm}$  at  $25^\circ\text{C}$  can be reduced by incorporating metal nanoparticles into the  $\text{TiO}_2$  matrix. Electrically conducting particles can be randomly distributed within a semiconductor matrix to form a composite. This composite sample is non-conducting until the volume fraction of the conducting phase reaches the so-called percolation threshold. It has been experimentally and analytically shown that in a conductor/semiconductor composite with the conductor at or above a given volume fraction ( $\phi_i$ ), a network of conducting particles is established and thus the composite resistivity suddenly decreases. The most widely applied technique for the preparation of metal/ $\text{TiO}_2$  composite materials is the sol–gel process. This has been applied to the fabrication of an Ag-NP/ $\text{TiO}_2$  system by Li *et al.* [91]. They prepared a solution for fabricating Ag-NP/ $\text{TiO}_2$  composite thin films by mixing a sol–gel solution of titania for thin film fabrication with an 18 mol% silver nitrate solution; a 6 mol% ethanol solution of silver nitrate was also employed. The electrical resistivity of the resultant composite thin film with the highest concentration (18 mol%) of Ag nanoparticles was of the order of  $10^3 \Omega \text{ cm}$ . Because the sol–gel method used in these studies involves metalloxane polymer formation in the medium, and because poor miscibility of each component is inevitable, Li *et al.* reported that it was difficult to obtain a homogeneous solution for silver concentrations above 18 mol%. Therefore, a lower electrical resistivity of the composite thin film may be attained in the event that a solution with an

even higher volumetric fraction of Ag nanoparticles can be homogeneously mixed with the titania precursor solution. The electrical conductivity of the resultant films is largely dependent on the volumetric fraction, size, and connectivity of the Ag nanoparticles, and the homogeneity of the dispersed silver in the dielectric titania matrix [92-95].

Using the MPM, mixed precursor solutions for fabricating Ag-NP/TiO<sub>2</sub> composite thin films could be easily prepared. As a result, Ag-NP/TiO<sub>2</sub> composite thin films of Ag volumetric fractions from 0.03 to 0.68 were fabricated with heat-treatment of the mixed precursor films at 600°C in air. To obtain quantitative information about the effects of Ag nanoparticles on the electrical properties, the nanostructures of the films were examined by TEM. The TEM images films with  $\phi_{\text{Ag}}$  of 0.26, 0.30, and 0.55 are shown in Figures 12 (A), (B), and (C) respectively [9]. The presence and distribution of Ag nanoparticles (black dots) inside the TiO<sub>2</sub> film can be clearly seen. The percolation threshold of Ag nanoparticles in the titania thin film was found to be  $\phi_{\text{Ag}}$  0.30. It is near the percolation threshold, when Ag particles are still not totally connected, that increasing the  $\phi_{\text{Ag}}$  by adding a small amount of Ag nanoparticles helps to build the conductive network and reduce the resistivity of the composite. Therefore, the decrease in resistivity was attributed to a change in the Ag nanoparticles' size, shape, and center-to-center distance between the Ag nanoparticles. As the Ag volumetric fraction increased further from 0.27 to 0.55, the electrical resistivity decreased from 10<sup>-2</sup> to 10<sup>-5</sup> Ω cm, respectively. At  $\phi_{\text{Ag}}$  0.61 to 0.68, the resistivity increased from 10<sup>-5</sup> to 10<sup>-3</sup> Ω cm due to the inevitable increase in resistivity caused by agglomeration of the Ag particles. This study shows that the MPM, which offers excellent miscibility of the silver and titania precursor solutions, is effective at overcoming the miscibility limitations of the conventional sol-gel method and is necessary for fabricating composite thin films with large  $\phi_{\text{Ag}}$  values.

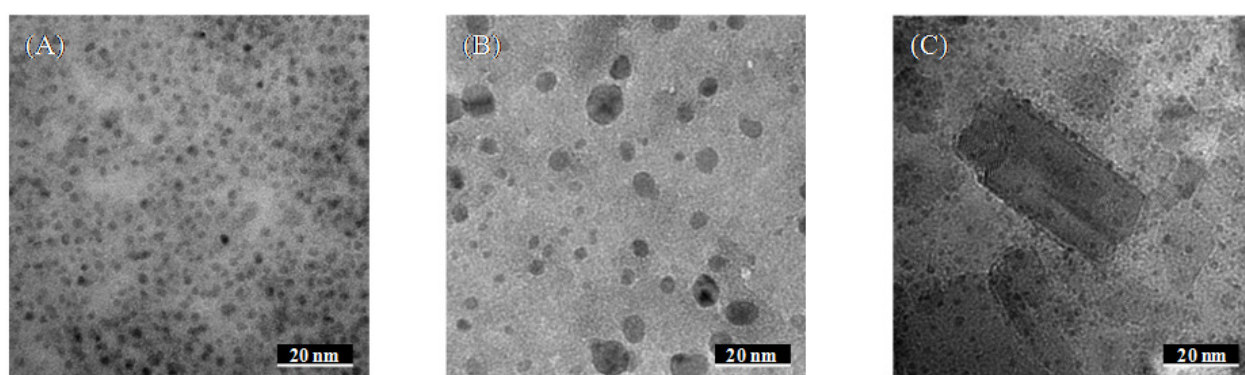


**Figure 12.** TEM images of the Ag-NP/TiO<sub>2</sub> composite thin films at Ag volumetric fractions,  $\phi_{\text{Ag}}$ , of (A) 0.26, (B) 0.30, and (C) 0.55, respectively [9].

The excellent miscibilities of the precursor complexes in the MPM overcame the limitations of the extremely low Ag volumetric fraction in the previous sol-gel process. Therefore, the percolation threshold for the electrical resistivity of the composite film could be examined for a wide range of Ag fractions. Heat-treatment plays an important role in the production of Ag nanoparticles by reducing Ag<sup>+</sup> ions in the precursor film and

forming well-dispersed Ag nanoparticles in the titania matrix. This present Ag-nanoparticle/titania composite thin film is useful for fabrication of highly conductive electrodes for devices such as solar cells.

## 10. Conclusion

The importance of heat-treatment in the MPM was demonstrated through fabrication of thin films of anatase and rutile with unprecedentedly high photoreactivities. This is due to a photoreactive mechanism via O deficiency in the oxide thin films. Based on the excellent miscibilities of the molecular precursors in the SrTiO<sub>3</sub> thin film fabrication, heat-treatment was shown to be an essential step. It eliminates organic ligands in the precursor metal complexes and provides important functions to the metal oxides in the chemical fabrication of Ag-nanoparticle/titania composite thin films with high conductivity.

The chemical fabrication of the first p-type Cu<sub>2</sub>O transparent thin film was also recently achieved using the MPM, although the heat-treatment of the spin-coated substrates resulted in the deposition of a large amount of powder on the substrates in previous sol-gel studies [96]. The electrical and optical properties of the Cu<sub>2</sub>O thin film fabricated using the MPM were consistent with those of similar thin films fabricated using physical procedures. It is very interesting that the charge on copper changes stepwise from +2 to +1 through 0 during heat-treatment of the precursor film involving a Cu-EDTA complex in an Ar gas flow. Based on these results, a transparent dry-type solar cell of area 20 × 20 mm<sup>2</sup> with a combination of Vis-responsive anatase thin films was examined. This film is mentioned in the section **Vis-responsive anatase thin film fabricated using the MPM**. The structure of the solar cell was FTO electrode/n-Vis-responsive anatase/p-Cu<sub>2</sub>O/conductive polymer/Ag on a glass substrate, and the photovoltaic nature of the solar cell could be successfully measured under the light from a solar simulator. Thus, the present MPM is useful for fabricating Vis-responsive dry solar cells. The MPM coupled with heat-treatment of various precursor films allows transparent thin films of metal oxides such as Co<sub>3</sub>O<sub>4</sub>, ZnO, Ga<sub>2</sub>O<sub>3</sub>, and ZrO<sub>2</sub> *etc.* to be examined and fabricated on glass and/or metallic substrates. The MPM has great potential as a fundamental technology for thin film fabrication by chemical processes.

## Author details

Hiroki Nagai and Mitsunobu Sato

*Research Institute of Science and Technology, Kogakuin University, Nakano, Hachioji, Tokyo, Japan*

## Acknowledgement

This work was supported by MEXT\*-Supported Program for the Strategic Research Foundation at Private Universities, 2011-2015 (Kogakuin University–Energy Conversion Ecomaterials Center). \*Ministry of Education, Culture, Sports, Science and Technology

## 11. References

- [1] Sato M, Hara H, Nishide T and Sawada Y (1996) A Water-resistant Precursor in a Wet Process for TiO<sub>2</sub> Thin Film Formation. *J. Mater. Chem.* 6: 1767-1770.
- [2] Nishide T, Sato M, Hara H (2000) Crystal Structure and Optical Property of TiO<sub>2</sub> Gels and Films Prepared from Ti-edta Complexes as Titania Precursors. *J. Mater. Sci.* 35: 465-469.
- [3] Sato M, Hara H, Kuritani M, Nishide T (1997) Novel Route to Co<sub>3</sub>O<sub>4</sub> Thin Films on Glass Substrates via N-alkyl Substituted Amine Salt of Co(III)-EDTA Complex. *Sol. Energy Mater. Sol. Cells* 45: 43-49.
- [4] Sato M, Tanji T, Hara H, Nishide T, Sakashita Y (1999) SrTiO<sub>3</sub> Film Fabrication and Powder Synthesis from a Non-polymerized Precursor System of a Stable Ti(IV) Complex and Sr(II) Salt of edta. *J. Mater. Chem.* 9: 1539-1542.
- [5] Nagai H, Mochizuki C, Hara H, Takano I, Sato M (2008) Enhanced UV-sensitivity of Vis-responsive Anatase Thin Films Fabricated by Using Precursor Solutions Involving Ti Complexes. *Sol. Energy Mater. Sol. Cells* 92: 1136-1144.
- [6] Nagai H, Hasegawa M, Hara H, Mochizuki C, Takano I, Sato M (2008) An Important Factor Controlling the Photoreactivity of Titania: O-deficiency of Anatase Thin Film. *J. Mater. Sci.* 43: 6902-6911.
- [7] Nagai H, Aoyama S, Hara H, Mochizuki C, Takano I, Baba N, Sato M (2009) Rutile Thin Film Responsive to Visible Light and with High UV Light Sensitivity. *J. Mater. Sci.* 44: 861-868.
- [8] Nagai H, Aoyama S, Hara H, Mochizuki C, Takano I, Honda T, Sato M (2010) Photoluminescence and Photoreactivity Affected by Oxygen Defects in Crystal-oriented Rutile Thin Film Fabricated by Molecular Precursor Method. *J. Mater. Sci.* 45: 5704-5710.
- [9] Likius DS, Nagai H, Aoyama S, Mochizuki C, Hara H, Baba N, Sato M (2012) Percolation Threshold for Electrical Resistivity of Ag-nanoparticle/Titania Composite Thin Films Fabricated Using Molecular Precursor Method. *J. Mater. Sci.* 47: 3890-3899.
- [10] Mochizuki C, Sasaki Y, Hara H, Sato M, Hayakawa T, Yang F, Hu X, Shen H, Wang S (2009) Crystallinity Control of Apatite through Ca-EDTA Complexes and Porous Composites with PLGA. *J. Biomed. Mater. Res. Part B* 90: 290-301.
- [11] Honda T, Oda T, Mashiyama Y, Hara H, Sato M (2010) Fabrication of c-axis Oriented Ga-doped MgZnO-based UV Transparent Electrodes by Molecular Precursor Method. *Phys. Status. Solidi.* 7: 2471-2473.
- [12] Twite RL, Bierwagen GP (1998) Review of Alternatives to Chromate for Corrosion Protection of Aluminum Aerospace Alloys. *Prog. Org. Coat.* 33: 91-100.
- [13] Neto DLP, Atik M, Avaca LA, Aegerter MA (1994) Sol-Gel ZrO<sub>2</sub> Coatings for Chemical Protection of Stainless Steel. *J. Sol-Gel Sci. Technol.* 1: 177-184.
- [14] Metroke TL, Parkhill RL, Knobbe ET (2001) Passivation of Metal Alloys Using Sol-gel-derived Materials-A review. *Prog. Org. Coat.* 41: 233-238.
- [15] Atik M, Neto DLP, Aegerter MA, Avaca LA (1995) Sol-gel TiO<sub>2</sub>-SiO<sub>2</sub> Films as Protective Coatings Against Corrosion of 316L Stainless Steel in H<sub>2</sub>SO<sub>4</sub> Solutions. *J. Appl. Electrochem.* 25: 142-148.

- [16] Wei Q, Narayan RJ, Narayan J, Sankar J, Sharma AK (1998) Improvement of Wear Resistance of Pulsed Laser Deposited Diamond-like Carbon Films through Incorporation of Metals. *Mater. Sci. Eng. B* 53: 262-266.
- [17] Wei Q, Sharma AK, Sankar J, Narayan J (1999) Mechanical Properties of Diamond-like Carbon Composite Thin Films Prepared by Pulsed Laser Deposition. *Compos. Part B: Eng.* 30: 675-684.
- [18] Nomura K, Ohta H, Takagi A, Kamiya T, Hirano M, Hosono H (2004) Room-temperature Fabrication of Transparent Flexible Thin-film Transistors Using Amorphous Oxide Semiconductors. *Nature* 432: 488-492.
- [19] Hoffman RL, Norris BJ, Wager JF (2003) ZnO-based Transparent Thin-film Transistors. *Appl. Phys. Lett.* 82: 733-735.
- [20] Tsukazaki A, Ohtomo A, Onuma T, Ohtani M, Makino T, Sumiya M, Ohtani K, Chichibu SF, Fuke S, Segawa Y, Ohno H, Koinuma H, Kawasaki M (2005) Repeated Temperature Modulation Epitaxy for p-type Doping and Light-emitting Diode Based on ZnO. *Nature Mater.* 4: 42-45.
- [21] Kim JH, Lee S, Im HS (1999) The Effect of Target Density and Its Morphology on TiO<sub>2</sub> Thin Films Grown on Si (100) by PLD. *Appl. Surf. Sci.* 151: 6-16.
- [22] Walczak M, Oujja M, Marco JF, Sanz M, Castillejo M (2008) Pulsed Laser Deposition of TiO<sub>2</sub>: Diagnostic of the Plume and Characterization of Nanostructured Deposits. *Appl. Phys. A* 93: 735-740.
- [23] Tang H, Prasad K, Sanjines R, Schmid PE, Levy F (1994) Electrical and Optical Properties of TiO<sub>2</sub> Anatase Thin Films. *J. Appl. Phys.* 75: 2042-2047.
- [24] Campbell SA, Kim HS, Gilmer DC, He B, Ma T, Gladfelter WL (1999) Titanium Dioxide (TiO<sub>2</sub>)-based Gate Insulators. *IBM. J. Res. Dev.* 43: 383-392.
- [25] Wang Z, Helmersson U, Kall PO (2002) Optical Properties of Anatase TiO<sub>2</sub> Thin Films Prepared by Aqueous Sol-gel Process at Low Temperature. *Thin Solid Films* 405: 50-54.
- [26] Sakka S (1994) The Current State of Sol-gel Technology. *J. Sol-Gel Sci. Technol.* 3: 69-81.
- [27] Sakka S (1982) Gel Method for Making Glass. *Treatise Mater. Sci. Technol.* 22: 129-167.
- [28] Sakka S (1988) *Science of Sol-Gel Method*. Tokyo: Agne-Shofu-Sha. 221 p.
- [29] Brinker CJ, Scherer GW (1990) *Sol-Gel Science*. New York: Academic Press. 908 p.
- [30] Hench LL, West JK (1990) The Sol-Gel Process. *Chem. Rev.* 90: 33-72.
- [31] Mazdiyasi KS, Dolloff RT, Smith JS (1969) Preparation of High-Purity Submicron Barium Titanate Powders. *J. Am. Ceram. Soc.* 52: 523-526.
- [32] Sakka S, Kamiya K (1982) The Sol-gel Transition in the Hydrolysis of Metal Alkoxides in Relation to the Formation of Glass Fibers and Films. *J. Non-Cryst. Solids* 48: 31-46.
- [33] Hu L, Yoko T, Kozuka H, Sakka S (1992) Effects of Solvent on Properties of Sol-gel-derived TiO<sub>2</sub> Coating Films. *Thin Solid Films* 219: 18-23.
- [34] Dimitriev Y, Ivanova Y, Iordanova R (2008) History of Sol-gel Science and Technology. *J. Univer. Chem. Technol. Metall.* 43: 181-192.
- [35] Hashimoto K, Irie H, Fujishima A (2007) TiO<sub>2</sub> Photocatalysis: A Historical Overview and Future Prospects. *AAAPS. Buliten.* 17: 12-28.
- [36] Fujishima A, Honda K (1972) Electrochemical Photolysis of Water at a Semiconductor Electrode. *Nature* 238: 37-38.

- [37] Pelizzetti E, Serpone N (Eds.) (1986) *Homogeneous and Heterogeneous Photocatalysis*. Dordrecht: D. Reidel Publishing Company. 752 p.
- [38] Serpone N, Pelizzetti E (Eds.) (1989) *Photocatalysis, Fundamentals and Applications*. New York: John Wiley & Sons. 650 p.
- [39] Kamat PV (1993) Photochemistry on Nonreactive and Reactive (Semi-conductor) Surfaces. *Chem. Rev.* 93: 267-300.
- [40] Ollis DF, Al-Ekabi H (Eds.) (1993) *Photocatalytic Purification and Treatment of Water and Air*. Amsterdam: Elsevier. 820 p.
- [41] Heller A (1995) Chemistry and Applications of Photocatalytic Oxidation of Thin Organic Films. *Acc. Chem. Res.* 28: 503-508.
- [42] Hoffmann MR, Martin ST, Choi W, Bahnemann DW (1995) Environmental Applications of Semiconductor Photocatalysis. *Chem. Rev.* 95: 69-96.
- [43] Mills A, Lehnste S (1997) An Overview of Semiconductor Photocatalysis. *J. Photochem. Photobiol. A: Chem.* 108: 1-35.
- [44] Peral J, Domènech X, Ollis DF (1997) Heterogeneous Photocatalysis for Purification, Decontamination and Deodorization of Air. *J. Chem. Tech. Biotech.* 70: 117-140.
- [45] Fujishima A, Hashimoto K, Watanabe T (1999) *TiO<sub>2</sub> Photocatalysis: Fundamentals and Applications*. Tokyo: BKC, Inc. 184 p.
- [46] Fujishima A, Rao TN, Tryk DA (2000) Titanium Dioxide Photocatalysis. *J. Photochem. Photobiol. C 1*: 1-21.
- [47] Ollis DF (2000) Photocatalytic Purification and Remediation of Contaminated Air and Water. *C. R. Acad. Sci. Paris, Serie II C, Chim.* 3: 405-411.
- [48] Tryk DA, Fujishima A, Honda K (2000) Recent Topics in Photoelectrochemistry: Achievements and Future Prospects. *Electrochim. Acta.* 45: 2363-2376.
- [49] Fujishima A, Tryk DA, Bard AJ, Stratmann M, Licht S (Eds.) (2002) *Encyclopedia of Electrochemistry, Vol. 6: Semiconductor Electrodes and Photoelectrochemistry*. Wiley-VCH: Weinheim. 608 p.
- [50] Hashimoto K, Irie H, Fujishima A (2005) *TiO<sub>2</sub> Photocatalysis: A Historical Overview and Future Prospects*. *Japan. J. Appl. Phys.* 44: 8269-8285.
- [51] Fujishima A, Zhang X (2006) *Titanium Dioxide Photocatalysis: Present Situation and Future Approaches*. *C. R. Chimie.* 9: 750-760.
- [52] Fujishima A, Zhang X, Tryk DA (2007) *Heterogeneous Photocatalysis: From Water Photolysis to Applications in Environmental Cleanup*. *Internat. J. Hydrogen Energy.* 32: 2664-2672.
- [53] Jacoby WA, Maness PC, Wolfrum EJ, Blake DM, Fennel JA (1998) Mineralization of Bacterial Cell Mass on a Photocatalytic Surface in Air. *Environ. Sci. Technol.* 32: 2650-2653.
- [54] Sunada K, Watanabe T, Hashimoto K (2003) Bactericidal Activity of Copper-deposited TiO<sub>2</sub> Thin Film under Weak UV Light Illumination. *Environ. Sci. Technol.* 37: 4785-4789.
- [55] Herrmann JM, Mozzanega MN, Pichat P (1983) Oxidation of Oxalic Acid in Aqueous Suspensions of Semiconductors Illuminated with UV or Visible Light. *J. Photochem.* 22: 333-343.

- [56] Herrmann JM, Disdier J, Pichat P (1984) Effect of Chromium Doping on the Electrical and Catalytic properties of Powder Titania under UV and Visible Illumination. *Chem. Phys. Lett.* 108: 618-622.
- [57] Pichat P, Herrmann JM, Disdier J, Mozzanega M, Courbon H (1984) Modification of the TiO<sub>2</sub> Electron Density by Ion Doping or Metal Deposit and Consequences for Photoassisted Reactions. *Stud. Surf. Sci. Catal.* 19: 319-326.
- [58] Serpone N, Lawless D, Disdier J, Herrmann JM (1994) Spectroscopic Photoconductivity, and Photocatalytic Studies of TiO<sub>2</sub> Colloids: Naked and with the Lattice Doped with Cr<sup>3+</sup>, Fe<sup>3+</sup>, and V<sup>5+</sup> Cations. *Langmuir.* 10: 643-652.
- [59] Ikeda S, Sugiyama N, Pal B, Marci G, Palmisano L, Noguchi H, Uosaki K, Ohtani B (2001) Photocatalytic Activity of Transition-metal-loaded Titanium (IV) Oxide Powders Suspended in Aqueous Solutions: Correlation with Electron-hole Recombination Kinetics. *Phys. Chem. Chem. Phys.* 3: 267-273.
- [60] Karvinen S, Hirva P, Pakkanen TA (2003) Ab Initio Quantum Chemical Studies of Cluster Models for Doped Anatase and Rutile TiO<sub>2</sub>. *J. Mol. Struct. Theochem.* 626: 271-277.
- [61] Zhu J, Deng Z, Chen F, Zhang J, Chen H, Anpo M, Huang J, Zhang L (2006) Hydrothermal Doping Method for Preparation of Cr<sup>3+</sup>-TiO<sub>2</sub> Photocatalysts with Concentration Gradient Distribution of Cr<sup>3+</sup>. *Appl. Catal. B-Eviron.* 62: 329-335.
- [62] Yamashita H, Honda M, Harada M, Ichihashi Y, Anpo M, Hatano Y (1998) Preparation of Titanium Oxide Photocatalysts Anchored on Porous Silica Glass by a Metal ion-implantation Method and Their Photocatalytic Reactivities for the Degradation of 2-propanol Diluted in Water. *J. Phys. Chem. B.* 102: 10707-10711.
- [63] Anpo M, Ichihashi Y, Takeuchi M, Yamashita H (1998) Design of Unique Titanium Oxide Photocatalysts by an Advanced Metal Ion-implantation Method and Photocatalytic Reactions under Visible Light Irradiation. *Res. Chem. Intermed.* 24: 143-149.
- [64] Anpo M, Kishiguchi S, Ichihashi Y, Takeuchi M, Yamashita H, Ikeue K, Morin B, Davidson A, Che M (2001) The Design and Development of Second-Generation Titanium Oxide Photocatalysts Able to Operate Under Visible Light Irradiation by Applying a Metal Ion-Implantation Method. *Res. Chem. Intermed.* 27: 459-467.
- [65] Anpo M (2004) Preparation, Characterization, and Reactivities of Highly Functional Titanium Oxide-based Photocatalysts Able to Operate under UV-Visible Light Irradiation: Approaches in Realizing High Efficiency in the Use of Visible Light. *Bull. Chem. Soc. Jpn.* 77: 1427-1442.
- [66] Anpo M, Takeuchi M, (1998) The Design and Development of Highly Reactive Titanium Oxide Photocatalysts Operating under Visible Light Irradiation. *J. Catal.* 216: 505-516.
- [67] Yamashita H, Harada M, Misaka J, Takeuchi M, Neppolian B, Anpo M (2003) Photocatalytic Degradation of Organic Compounds Diluted in Water Using Visible light-responsive Metal Ion-implanted TiO<sub>2</sub> Catalysts: Fe Ion-implanted TiO<sub>2</sub>. *Catal. Today.* 84: 191-196.
- [68] Asahi R, Morikawa T, Ohwaki T, Aoki K, Taga Y (2001) Visible-light Photocatalysis in Nitrogen-doped Titanium Oxides. *Science* 293: 269-271.

- [69] Miyauchi M, Ikezawa A, Tobimatsu H, Irie H, Hashimoto K (2004) Zeta Potential and Photocatalytic Activity of Nitrogen Doped TiO<sub>2</sub> Thin Films. *Phys. Chem. Chem. Phys.* 6: 865-870.
- [70] Valentin C, Finazzi E, Pacchioni G, Selloni A, Livraghi S, Paganini CM and Giamello E (2007) N-doped TiO<sub>2</sub>: Theory and Experiment. *Chem. Phys.* 339: 44-56.
- [71] Sathish M, Viswanathan B, Viswanath RP and Gopinath CS (2005) Synthesis, Characterization, Electronic Structure, and Photocatalytic Activity of Nitrogen-Doped TiO<sub>2</sub> Nanocatalyst. *Chem. Mater.* 17: 6349-6353.
- [72] Chen X, Burda B (2004) Photoelectron Spectroscopic Investigation of Nitrogen-Doped Titania Nanoparticles. *J. Phys. Chem.* 108: 15446-15449.
- [73] Saha NC, Tompkins HG, (1992) Titanium Nitride Oxidation Chemistry - An X-ray Photoelectron Spectroscopy. *J. Appl. Phys.* 72: 3072-3079.
- [74] Valentin DC, Pacchioni G, Selloni A, Livraghi S, Giamello E (2005) Characterization of Paramagnetic Species in N-doped TiO<sub>2</sub> powders by EPR Spectroscopy and DFT Calculations. *J. Phys. Chem. B* 109: 11414-11419.
- [75] Li FB, Li XZ (2002) Photocatalytic Properties of Gold/Gold Ion-modified Titanium Dioxide for Wastewater Treatment. *Appl. Catal. A* 228:15-27.
- [76] Tang J, Zou Z, Yin J, Ye J (2003) Photocatalytic Degradation of Methyleneblue on CaIn<sub>2</sub>O<sub>4</sub> under Visible Light Irradiation. *Chem. Phys. Lett.* 382: 175-179.
- [77] Kwon CH, Kim JH, Jung IS, Shin H, Yoon KH (2003) Preparation and Characterization of TiO<sub>2</sub>-SiO<sub>2</sub> Nano-composite Thin Films. *Ceram. Int.* 29: 851-856.
- [78] Yu JC, Yu J, Zhang L, Ho W (2002) Enhancing Effects of Water Content and Ultrasonic Irradiation on the Photocatalytic Activity of Nano-sized TiO<sub>2</sub> Powders. *J. Photochem. Photobiol. A* 148: 263-271.
- [79] Kominami H, Kato J, Murakami S, Kera Y, Inoue M, Inui T, Ohtani B (1999) Synthesis of Titanium (IV) Oxide of Ultra-high Photocatalytic Activity: Hydrolysis of Titanium Alkoxides with Water Liberated Homogeneously from Solvent Alcohols. *J. Mol. Catal. A. Chem.* 144: 165-171.
- [80] Fackler Jr JP, Kristine FJ, Mazany AM, Moyer TJ, Shepherd RE (1985) The Absence of a Titanium Oxygen in the Titanium(IV)ethylenediaminetetraacetate(4-) Complex: [Ti(edta)(H<sub>2</sub>O)]. *Inorg. Chem.* 24: 1857-1860.
- [81] Nishimoto S, Ohtani B, Kajiwarra H, Kagiya T (1985) Correlation of the Crystal Structure of Titanium Dioxide Prepared from Titanium Tetra-2-propoxide with the Photocatalytic Activity for Redox Reactions in Aqueous Propanol and Silver Salt Solutions. *J. Chem. Soc. Faraday. Trans.* 81: 61-68.
- [82] Follis D, Pelizzetti E, Serpone N (1991) Photocatalyzed Destruction of Water Contaminants. *Environ. Sci. Technol.* 25: 1523-1529.
- [83] Fox MA, Dulay MT (1993) Heterogeneous Photocatalysis. *Chem. Rev.* 83: 341-356.
- [84] Robert DS, Pask AJ (1965) Kinetics of the Anatase-Rutile Transformation. *J. Am. Ceram. Soc.* 48: 391-398.
- [85] Dorian AH, Hanaor and Charles CS (2011) Review of the Anatase to Rutile Phase Transformation. *J. Mater. Sci.* 46: 855-874.

- [86] Jung KY, Park SB (1999) Anatase-phase Titania: Preparation by Embedding Silica and Photocatalytic Activity for the Decomposition of Trichloroethylene. *J. Photochem. Photobiol. A* 127: 117-122.
- [87] Lotgering FK (1959) Topotactical Reactions with Ferromagnetic Oxides Having Hexagonal Crystal Structures-I. *J. Inorg. Nucl. Chem.* 9: 113-123.
- [88] Nikilić LM, Radonjić L, Srđić VV (2005) Effect of Substrate Type on Nanostructured Titania Sol-gel Coatings for Sensors Applications. *Ceram. Inter.* 31: 261-266.
- [89] Yamashita H, Ichihashi Y, Zhang SG, Matumura Y, Souma Y, Tatsumi T, Anpo M (1997) Photocatalytic Decomposition of NO at 275 K on Titanium Oxide Catalysts Anchored within Zeolite Cavities and Framework. *Appl. Surf. Sci.* 121/122: 305-309.
- [90] Nakamura R, Okamura T, Ohashi N, Imanishi A, Nakato Y (2005) Molecular Mechanisms of Photoinduced Oxygen Evolution, PL Emission, and Surface Roughening at Atomically Smooth (110) and (100) n-TiO<sub>2</sub> (Rutile) Surfaces in Aqueous Acidic Solutions. *J. Am. Chem. Soc.* 127: 12975-12983.
- [91] Li H, Zhao G, Song B, Han G (2008) Effect of Incorporation of Silver on the Electrical Properties of Sol-gel-derived Titania Film. *J. Cluster Sci.* 19: 667-673.
- [92] Ambrozic M, Dakskobler A, Valant M, Kosmac T (2005) Percolation Threshold Model and Its Application to the Electrical Conductivity of Layered BaTiO<sub>3</sub>-Ni. *Mater. Sci-Pol.* 23: 535-539.
- [93] Lo CT, Chou K, Chin W (2001) Effects of Mixing Procedures on the Volume Fraction of Silver Particles in Conductive Adhesives. *J. Adhes. Sci. Technol.* 15: 783-792.
- [94] Sancaktar E, Bai L (2011) Electrically Conductive Epoxy Adhesives. *Polymers* 3: 427-466.
- [95] Ren P, Fan H, Wang X, Shi J (2011) Effects of Silver Addition on Microstructure and Electrical Properties of Barium Titanate Ceramics. *J. Alloy. Compd.* 509: 6423-6426.
- [96] Armelao L, Barreca D, Bertapelle M, Bottaro G, Sada C, Tondello E (2003) A sol-gel approach to nanophasic copper oxide thin films. *Thin Solid Films* 442: 48-52.